euspen's 20th International Conference & Exhibition, Geneva, CH, June 2020

www.euspen.eu

Development of thermal nanospectroscopic system for THz evanescent wave

Ryoko Sakuma[1*], Kuan-Ting- Lin[2], Sunmi Kim[2,3], Fuminobu Kimura[1,2], Yusuke Kajihara[1,2]

[1]*Department of Precision Engineering, The University of Tokyo, Hongo 7-3-1, Bunkyo-ku, Tokyo 113-8656, JAPAN*
[2]*Institute of Industrial Science, The University of Tokyo, Komaba 4-6-1, Meguro-ku, 153-8505, Japan*
[3]*National Institute of Information and Communications Technology, Nukui-Kitamachi 4-2-1, Koganei, Tokyo 184-8795, Japan*

**Submitting author: sakumar@iis.u-tokyo.ac.jp*

Abstract

All materials are covered by strongly localised surface evanescent waves induced by charge polarisation due to local phenomena of materials such as electron movement, lattice vibration, and molecular motion. The surface wave spectra lie in the terahertz (THz) region (wavelength: 8-20 μm) at room temperature, which makes it a rich information source of materials. To detect such spontaneous surface waves without any influences from the external environment, we have developed passive scattering-type scanning near-field optical microscopy (passive s-SNOM). It achieved THz evanescent waves on metals and dielectrics with a spatial resolution of 20 nm at the wavelength of 14.5 μm without any external illumination. However, a narrow detectable wavelength range of the passive s-SNOM (14.5 ± 0.8 μm) largely limits the observable materials. To improve the passive s-SNOM into a widely used nanoscale chemical/thermal microscopy, we intend to develop a passive THz nano-spectroscopic system. The spectroscopic system was build based on grating type spectroscopy in the 4.2 K cryostat, and the wavelength range was extended to 8 – 16 μm using a recently developed ultra-sensitive infrared detector, three-colour charge sensitive infrared phototransistor (CSIP). It selects a wavelength by rotating the grating by piezoelectric rotary motor and detects only the first-order diffraction light. The grating structure was designed to have maximum diffraction efficiency over the three-colour CSIP detectable wavelengths and was machined with a super-precise cutting machine. The diffraction performance of the machined grating and the rotational accuracy of the rotary motor at 4.2 k temperature were evaluated, and their performances showed that they were sufficient enough (within 5 % error of diffraction efficiency and 2 % rotation error at 4.2 K) to perform spectroscopic analysis. Here, we report the spectral performance of this passive THz spectroscopic system. This is a first attempt to get a passive nanoscale THz spectrum at room temperature.

Keywords: Measurement, Nano technology, Optical, Scanning probe microscope (SPM)

1. Introduction

Thermal analysis on an electrical component is required in nanoscale due to the miniaturisation of devices. Thermal energy corresponds to electromagnetic waves with THz frequency, according to the theory of density of emitted electromagnetic energy [1]. On the material surface, the thermal energy excites local phenomena such as electron movement and lattice vibration. It induces nanoscale non-uniform charge distribution and localise strong electromagnetic wave called surface evanescent wave within 100 nm above the material surface.

In order to analyse the thermal distribution of the miniaturised devices, a nano-scale passive-type measuring technique is indispensable. The passive type measuring technique does not use any external light sources and detect electromagnetic waves directly from the sample. It allows to detect electromagnetic waves induced by the local phenomena of materials, giving us information of the local states of phenomena [2]. The popular passive measurement technique is the thermography [3], which detects infrared waves directly from the target object to map a temperature distribution.

To detect the electromagnetic wave induced by the local phenomena passively, we have developed passive THz scattering-type scanning near-field optical microscopy (s-SNOM), shown in Fig. 1(a), which consists of an ultra-sensitive infrared detector, charge sensitive infrared phototransistor (CSIP) [4, 5], a confocal optical system with a pinhole of 125 μm diameter, and a homemade AFM [6, 7]. The scattered light by the AFM probe is collected by the Ge objective and then incidents on the detector CSIP. The CSIP is fabricated in a GaAs/AlGaAs double quantum well crystal (see Fig. 1(b)), and has an upper quantum well (UQW) and a lower quantum well (LWQ). Electrons in the electrically isolated UQW are excited by the incident photons via intersubband transition on the coupler gate (CG) and tunnel to the LQW. The signal is detected as a magnified current through the LQW and has a high sensitivity of NEP of 7×10^{-20} W $Hz^{1/2}$. The passive s-SNOM has achieved the imaging of THz evanescent wave on dielectric and metal materials with a spatial resolution of 20 nm at the wavelength of 14.5 μm [8]. The passive s-SNOM is the only technique for passively detecting the surface evanescent wave with a spatial resolution of tens of nanometre. It is applied to image electron fluctuation distribution [9] and nano-scale local heating distribution [10].

However, the detectable wavelength of the passive s-SNOM is determined by the detector CSIP structure. A single wavelength (14.5 ± 0.8 μm, Figure 1(c)) was detected by the conventional passive THz s-SNOM. For further analysis of the nanoscale thermal energy, a multi-wavelength selective operation is essential. In this paper, we report a THz spectroscopic s-SNOM with newly developed grating-based spectroscopic system. The whole system was arranged to operate at a temperature of 4.2 K and has a multi-wavelengths selective mechanism with a wavelength resolution of 500 nm. The detectable wavelength range of the detector CSIP was extended to 8-16 μm, allowing this technique applicable to widely used THz spectroscopy. This is the first attempt to achieve nano-scale passive type

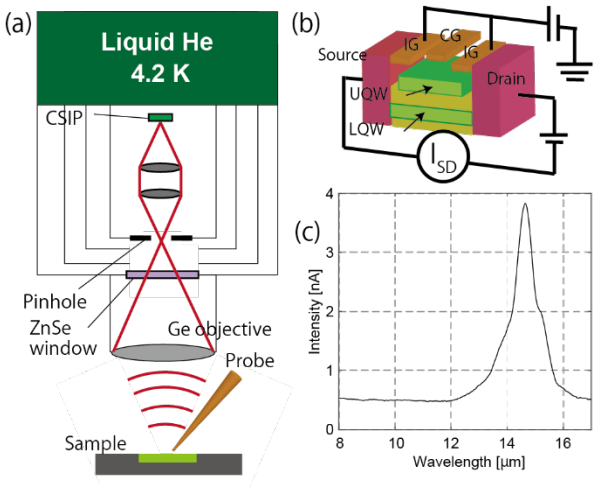

Figure 1. passive s-SNOM. (a) a schematic diagram of the passive s-SNOM. (b) Sensor CSIP structure. (c) Optical response of the CSIP

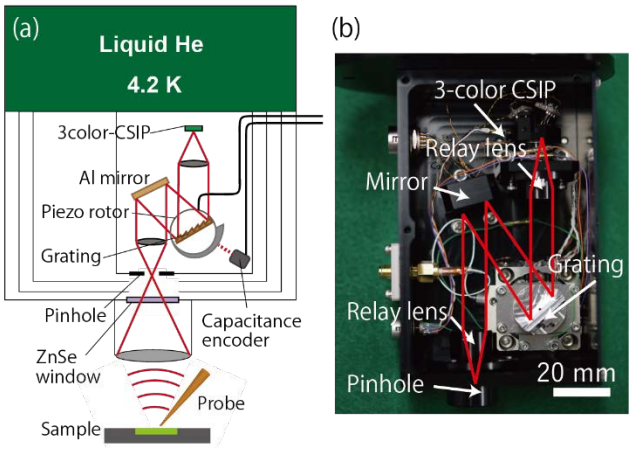

Figure 2. THz spectroscopic s-SNOM. (a) a schematic diagram (b) picture of the spectroscopic optical unit

spectroscopy in THz frequency range without heating the system. This passive THz spectroscopy will be applied to the nano-thermography or nano-chemical microscopy, measuring techniques that directly observe phenomena on materials with nano-scale spatial resolution.

2. Development of a grating-based spectroscopic system

The THz spectroscopic s-SNOM has designed to have an extended wavelength range and a multi-wavelengths selective mechanism. The multi-wavelengths selective mechanism was achieved with a grating-based spectroscopic system in which only the interference wavelength is selected. Figure 2 (a) is the schematic diagram of THz spectroscopic s-SNOM. Scattered evanescent waves by the probe apex are collected by the Ge objective lens. It is reflected by the Al mirror and incident to the Al grating at an incident angle of 30°. The whole spectroscopic system is in shielded rectangular box of 120 mm height, 70 mm width and 40 mm length as shown in Fig.2 (b). We intended to use the grating-based system rather than other spectroscopic techniques such as FTIR system [11] due to its high reflection efficiency, simple long-range wavelength control, and space limitation. All systems should operate at liquid helium temperature (4.2 K) to avoid excessive noise from the external environment at room temperature. It allows the detection of small signals by incident photons.

2.1. Extended wavelength range by three-colour CSIP

The wavelength range was extended by three-colour CSIP [12] which has three energy absorption peaks at the wavelength of 9.0, 11.7 and 14.5 μm. The three-colour CSIP consists of three UQWs and one LQW, where the conventional one-colour CSIP has one UQW and one LQW. The detectable wavelengths are determined by the thicknesses of the UQWs which are 7-8 nm. Figure 3 (a) shows the photo response of the three-colour CSIP. The combination of thee peaks has achieved the extended wavelength of 8-16 μm. However, since the UWQ corresponding to the wavelength of 14.5 μm is the third upper layer, the peak at the wavelength of 14.5 μm is weak and the photons are less likely to excite the UQW electron.

2.2. Calculation of the diffraction efficiency of a blazed grating

The spectroscopic property is mainly determined by the grating geometry. Based on the grating diffraction theory [13], the interference wavelength and the diffraction efficiency are determined by the pitch and the geometry of a grating. The common grating shapes are blazed (with rectangular apex, Fig 3(b)) and holographic. The different grating geometries have different diffraction efficiencies and optical properties. The blazed grating is highly efficient although the holographic grating is less efficient but contain less stray light. For the THz spectroscopic SNOM, we intended to use the blazed grating due to its high diffraction efficiency. The passively detected signals from most of materials are extremely weak and the multi-wavelengths selective mechanism makes the wavelength resolution smaller than the conventional s-SNOM. Therefore, the diffraction efficiency of grating should be designed to have high diffraction efficiency.

The blazed grating is required to have: 1) more than 60 % of diffraction efficiency for the first order diffraction light and 2) less than 10 % for the second order light over the wavelength range of 8-16 μm. The grating geometry that meets these requirements can select only the first order diffraction light. To perform reliable spectroscopic measurement, it is necessary to avoid mixing multiple wavelengths due to difference in the order of diffraction light.

The diffraction wavelength and efficiency were calculated based on the scalar theory of grating [14], which is an unpolarised approximate expression of infinite conductivity theory (the vector theory [15]), but has a high similarity to small blazed angles and small ratios of grating pitch to the wavelength. The diffraction wavelength λ with mth order light is

$$\lambda = d/m\ (\sin\theta_i + \sin(\theta_i + \phi)), \qquad (1)$$

where d, θ_i, and ϕ are the pitch, incident angle to the normal of the grating, and angle difference between incident and reflection light. ϕ in Eq. (1) is 30°, the area of CG of the sensor CSIP is approximately 100 μm square, and the focal length of the relay lens is 22.55 mm. Based on the geometric optics, we designed the grating system to have the wavelength resolution of 100 nm; therefore, the pitch of grating was determined to 15.5 μm.

The diffraction efficiency curve is determined by the blazed angle β shown in Fig.3 (b). If the blazed angle is small, a narrow efficiency peak is obtained at a short wavelength, and if the blazed grating is large, a wide peak is obtained at a long wavelength. The wavelength range of three-colour CSIP is 8 – 16 μm; therefore, the grating shape was designed to have maximized diffraction efficiency over the wavelength range of 8 – 16 μm. However, three lenses in the optical system have anti-reflection coating at the wavelength of 12 μm and 14 μm. It makes the transmittance rate lower at the shorter wavelength. Hence, the diffraction efficiency of the grating geometry was designed to have a maximum peak at a wavelength of 9 μm. The diffraction efficiency is given by

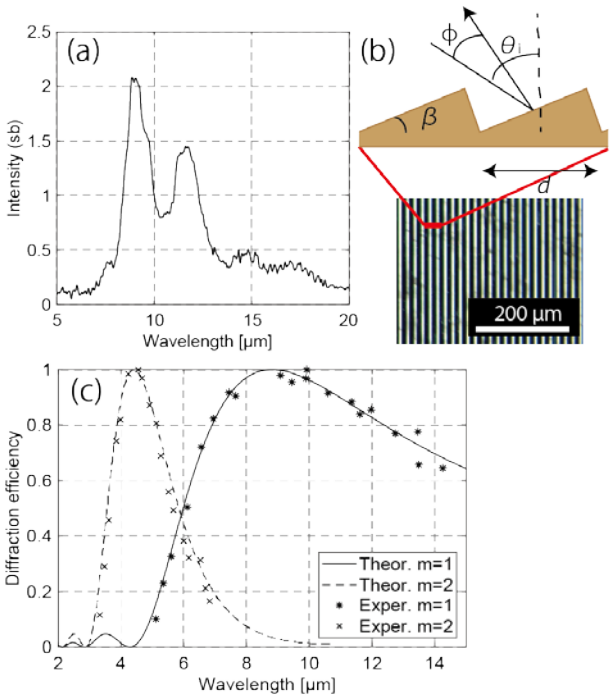

Figure 3. Optical property of THz spectroscopic s-SNOM. (a) Photo response of thee-colour CSIP (b) Cross section image and microscopic picture of fabricated blazed grating. (c) Diffraction efficiency of grating. Solid and dashed lines are the calculated efficiency and plotted points are the measured efficiency by FTIR.

$$I = sinc^2\left(\frac{\pi d}{\lambda}\frac{cos\theta_i}{\cos(\theta_i-\beta)} \cdot [\sin(\theta_i-\beta)+\sin(\theta_i+\phi-\beta)]\right). \quad (3)$$

The solid and dashed line in Fig. 3(c) are the calculated value of the first and the second order diffraction efficiency by Eq. (3). It has more than 62 % of first order diffraction light and less than 8 % of second order diffraction light.

2.3 FTIR analysis on the reflection efficiency

The brazed grating was machined by a super-precise cutting machine, ROBONANO (FANUC corp.). Figure 3(b) shows the microscopic image of machined grating, which has a cutting error within 0.3 %. Assuming the thermal shrinkage of aluminium at the temperature of 4.2 K, it was fabricated with the pitch of 15.61 μm.

The diffraction efficiency curve was experimentally obtained with FTIR. FTIR has an infrared light source with a wavelength of 1.4-15 μm. The wavelength longer than 15 μm cannot be obtained due to a low SN ratio of signals. The diffraction efficiency was calculated by taking the ratio of detected spectrum to the reference spectrum. The reference spectrum was obtained without any optics in the FTIR sample room. The efficiency of the second order diffraction light longer than 7.5 μm was not be obtained for the same reason as the first order diffraction light longer than 15 μm. The plotted points in Fig. 3(c) show the experimentally obtained diffraction efficiency. Both the first and the second order light have accuracies within 6 % to the calculated values. Over the 8 – 16 μm wavelength range, diffraction efficiency of the first and the second order diffraction light is expected to be more than 62 % and less than 8 % due to its high consistency with the theoretical value.

3. Rotation mechanism at liquid helium temperature

The spectroscopic SNOM optics are placed in a cryostat at a liquid helium temperature of 4.2 K. One of the mechanical

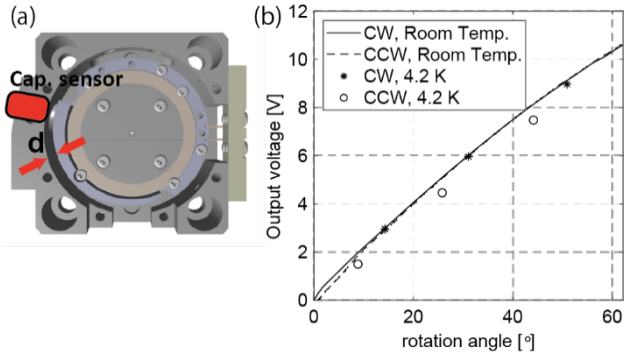

Figure 4. Piezoelectric rotor with capacitance rotation sensor (a) CAD image of piezoelectric rotor. The gap distance d changes by rotating the stage. (b) The output voltage of capacitance sensor with stage rotation. Solid and dashed lines are the output voltage of sensor with CW and CCW direction at room temperature. Plotted points are those of at temperature of 4.2 K.

actuators that properly operate at a temperature of 4.2 K is a piezoelectric rotor that utilises the rapid deformation of a piezoelectric crystal. By applying pulse voltage to control the contraction and elongation of the crystal, the stage can move in one dimension by friction force [16]. In order to apply this one-dimensional motion to the rotation motion, the stage is fixed to a free rotating ball bearing around a fixed rotation axis. Piezoelectric crystals are placed every 120°, making smooth rotation even at an ultra-low temperature.

Since the characteristics of a piezoelectric crystal at a temperature of 4.2 K are not the same as those at the room temperature [17], the spectroscopic system requires a rotation measuring mechanism. We develop the rotation stage with the capacitance sensor, shown in Fig.4 (a), which can measure the gap distance d by measuring its output voltage. The output voltage of the capacitance sensor is given by

$$V = Id/\omega\varepsilon A, \quad (4)$$

where ε and A are the dielectric constant and the sensing area. The gap distance was fabricated to have 500 μm change at 60° rotation.

Solid and dashed lines in Fig.4(b) indicate the output voltage of the capacitance sensor with the grating rotated CW and CCW direction at room temperature. The rotation angle was measured by a rotary encoder perpendicularly settled on the rotary stage. The output voltage and the rotation angle are theoretically linearly proportional according to Eq. (4); however, it is slightly quadratic due to the non-linearity of the gap distance. The output voltage changes by 10.4 V when rotated 60°. The plotted points shown as open and filled circles are the output voltage measured at a temperature of 4.2 K in the CW and CCW rotation direction respectively. The output voltage in the CW rotation was highly consistent with that at room temperature. It was within 0.1 V error. However, the rotation in the CCW direction has low accuracy, approximately 0.7 V systematic error. A difference of 0.1 V in the output voltage of the capacitance sensor corresponds to a rotation error of approximately 0.6° rotation error, which is a wavelength error of 300 nm according to Eq. (1). Therefore, only the CW rotation direction is used for the spectroscopic measurements.

4. Far-field THz spectroscopic analysis

A spectroscopic system with the diffraction grating and the piezoelectric rotor was cooled to a temperature of 4.2 K, and its photo response was measured with a thermal source at a temperature of approximately 500 K. The thermal source was placed at the focus position of the objective lenses which was 25

mm below the lens. The reflection efficiency of the Al mirror and the Al diffraction grating, shown in Fig.2 (a), was 80 % and 64 %, respectively. The grating position was properly adjusted to have maximum light efficiency with two screws on the back of the grating unit. The signal intensity was measured by calculating the current difference detected by CSIP when the thermal source was switched on and off every 5 seconds.

Figure 5 indicates the change in the far-field signal strength with one-colour CSIP and three-colour CSIP when the incident angle to the grating was gradually changed from 15° to 47°, corresponding to the wavelength change of 0 – 16 μm according to the Eq.(1). When the wavelength is equal to zero, a single strong peak was observed because the optical path difference is equal to zero at this specific incident angle. The wavelength shift was due to the offset of the initial grating angle. Using this unique incident angle, called all wavelength reflection angle, the offset of the grating angle can be calibrated. The wavelength resolution of this spectroscopic system was approximately 100 nm (see section 2.2); however, the experimentally absorbed wavelength resolution was about 500 nm, according to the FWHM of the peak at the all wavelength reflection angle. It was due to the unsharpened rectangular apex of the blazed grating and small differences in the grating pitches.

This spectroscopic system was built to have the wavelength range of 8 – 16 μm, the wavelength range of the three-colour CSIP; however, the signal intensity of the spectroscopic s-SNOM with the three-colour CSIP was extremely small comparing to that with the one-colour CSIP. There are mainly two reasons. First, the transmittable wavelength range of the Ge objective is narrow due to the antireflection coating at the wavelength of 14.5 μm. The first and second energy peaks of the three-colour CSIP (wavelength: 9.0 μm and 11.7 μm) are large enough; however, they are mostly diminished, making the detectable wavelength range to 10.5 – 16 μm. In the case of one-colour CSIP, the energy peaks at a wavelength of 14.5 μm (see Fig. 3(a)) is narrow but strong, which is about 3.3 nA. The antireflection coating of the Ge objective at a wavelength of 14 μm does not significantly affect the photo-response of the one-colour CSIP. Therefore, together with the antireflection coating and the weak energy peak at a wavelength of 14.5 μm, the signal strength with three-colour CSIP is weaker than that with one-colour CSIP. However, the signal intensity with three-colour CSIP can be enlarged by lowering the wavelength of anti-reflection coating, which will be achieved in the near future. It will increase the signal intensity to several tens times larger than that shown in the Fig 5 (b). Then the passive s-SNOM with three-colour CSIP will be useful to perform the passive spectroscopic measurements of wide range of materials while that with one-colour CSIP is for the measurement on a specific material.

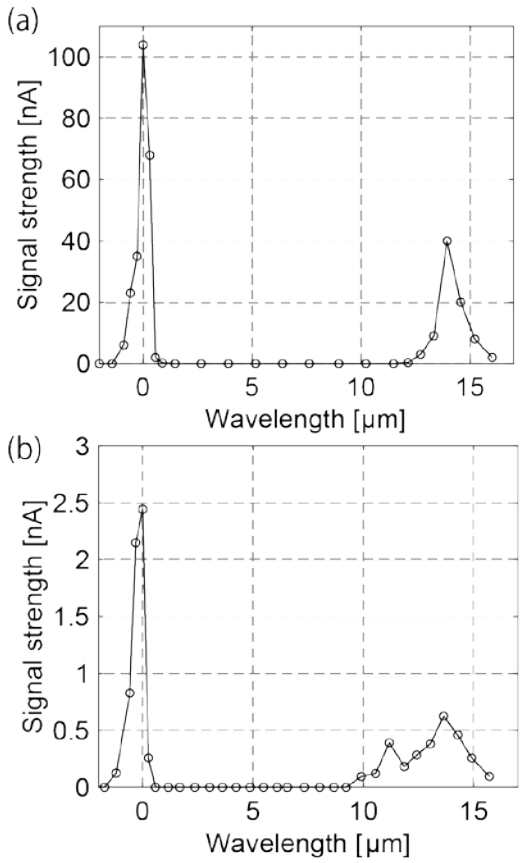

Figure 5. Far-field spectrum intensity of thermal sources with THz spectroscopic system. (a) with one-colour CSIP (b) with three-colour CSIP.

5. Summary

In this study, we developed a passive-type THz spectroscopy with a blazed grating and a piezoelectric rotary stage. The whole system is cooled down to a temperature of 4.2 K, thus it requires a spectroscopic system works properly at an ultra-low temperature. The blazed grating was designed to maximise diffraction efficiency at a wavelength range of 8 – 16 μm, and its performance has been demonstrated by the FTIR analysis. The rotation accuracy of the piezoelectric rotor at a temperature of 4.2 K was about 0.1 V compared to that at room temperature. Together with the blazed grating and the piezoelectric rotor, it has achieved the wavelength resolution of about 500 nm and multi-wavelengths selective mechanism at 4.2 K. The signal intensity with three-colour CSIP will be improved to several tens times larger by lowering the wavelength of anti-reflection coating in the near future. We are currently working on passive spectroscopic signal detection and it will be realised soon.

References

[1] Joulain K, Mulet J-P, Marquier F, Carminati R and Greffet J-J, 2005 *Surf. Sci. Rep.* **57** 59-112.
[2] Knoll B and Keilmann F, 1999 *Nature* **399** 134-137.
[3] Lahiri b B, Bagavathiappan S, Jayakumar T and Philip J, 2012 *Infrared Phys. Technol.* **55** 221-235.
[4] Komiyama S, 2011 *IEEE J. Sel. Top. Quantum Electron*. **17**(1) 54-66.
[5] Kajihara Y, Nakajima T, Wang Z and Komiyama S, 2013 J. Appl.Phys. **113** 136506
[6] Wang A, Komiyama S, Ueda T, and Nagai N, 2009 *Appl. Phys. Lett*. **95**(2) 022112.
[7] Kajihara Y, Kosaka K and Komiyama S, 2011 *Opt. Express* **19**(8) 7695-7704.
[8] Lin K-T, Komiyama S and Kajihara Y, 2016 *Opt. Lett*. **41**(3) 484-487.
[9] Weng Q, Komiyama S, Yang L, An Z, Chen P, Biehs S-A, Kajihara Y, Lu W, 2018 *Science* **360**(6390) 775-778.
[10] Weng Q, Lin K-T, Yoshida K, Nema H, Komiyama S, Kim S, Hirakawa K, and Kajihara Y, 2018 *Nano Lett*. **18**(7) 4220-4225.
[11] Huth F, Schnell M, Wittborn J, Ocelic N and Hillenbrand R, 2011 *Nat. Mater.* **10** 352-356.
[12] Kim S, Komiyama S, Ueda T, Satoh T and Kajihara Y, 2015 *Appl. Phys. Let.* **107** 182106.
[13] Loewen E G, Nevière M and Maystre D, 1977 *Appl. Opt.* **16**(10) 2711-2721.
[14] Casini R. and Nelson P G, 2014 *J. Opt. Soc. Am. A* **31**(10) 2179-2186.
[15] Petit R, 1975 *Nouv. Rev. Optique* **3** 129-135.
[16] Higuchi T, Yamagata Y, Furutani K and Kudoh K, 1990 *IEEE* 3776083.
[17] Litvin A F, Doroshenko V A, Gurtovoy V I and Pikalev M M, 1982 *Ferroelectrics* **41**(1) 163-168.